LAWRENCE
LIVERMORE
NATIONAL
LABORATORY

LLNL-JRNL-590393

An Experimental and Modeling Study Investigating the Ignition Delay in a Military Diesel Engine Running Hexadecane (Cetane) Fuel

J. S. Cowart, W. P. Fischer, L. J. Hamilton, P. A. Caton, S. M. Sarathy, W. J. Pitz

October 11, 2012

International Journal of Engine Research

Disclaimer

AN EXPERIMENTAL AND MODELING STUDY INVESTIGATING THE IGNITION DELAY IN A MILITARY DIESEL ENGINE RUNNING HEXADECANE (CETANE) FUEL

J. S. Cowart, W. P. Fischer, L. J. Hamilton and P. A. Caton

US Naval Academy, 121 Blake Rd, Annapolis, MD, USA

S. M. Sarathy and W. J. Pitz

Lawrence Livermore National Laboratory

Livermore, CA, USA

KEYWORDS

diesel, engine, fuel, ignition delay, hexadecane, cetane, combustion kinetics

ABSTRACT

In an effort aimed at predicting the combustion behavior of a new fuel in a conventional diesel engine, cetane (n-hexadecane) fuel was used in a military engine across the entire speed-load operating range. Ignition delay was characterized for this fuel at each operating condition. A chemical ignition delay was also predicted across the speed-load range using a detailed chemical kinetic mechanism with a constant pressure reactor model. At each operating condition the measured in-cylinder pressure and predicted temperature at the start of injection were applied to the detailed n-hexadecane kinetic mechanism, and the chemical ignition delay was predicted without any kinetic mechanism calibration. The modeling results show that fuel-air parcels developed from the diesel

spray with an equivalence ratio of four are the first to ignite. The chemical ignition delay results also showed decreasing igntion delays with increasing engine load and speed just as the experimental data revealed. At lower engine speeds and loads the kinetic modeling results show the characteristic two-stage NTC (Negative Temperature Coefficient) behavior of hydrocarbon fuels. However, at high engine speeds and loads the reactions do not display NTC behavior as the reactions proceed directly into high temperature pathways due to higher temperatures and pressure at injection. A moderate difference between the total and chemical ignition delays was then characterized as a phyical delay period which scales inversely with engine speed. This physical delay time is representative of the diesel spray development time and is seen to become a minority fraction of the total igntion delay at higher engine speeds. The approach used in this study suggests that the ignition delay and thus start of combustion may be predicted with reasonable accuracy using a kinetic modeling to determine the chemical igntion delay. Then, in conjunction with the physical delay time (experimental or modeling based) a new fuel's acceptability in a conventional engine could be assessed by determining that the total ignition delay is not too short or too long.

NOTATION

AOP	angle of peak
BMEP	brake mean effective pressure
BSFC	brake specific fuel consumption
BT	brake torque
BTC	before top center
C_2H_2	acetylene
C16	normal hexadecane

CAD	crank angle degree
CH_2O	formaldehyde
CO	carbon monoxide
CO_2	carbon dioxide
FMEP	friction mean effective pressure
FT	Fischer-Tropsch
GEP	General Engine Products
GTL	gas to liquid
H_2O_2	Hydrogen peroxide
HC	Hydrocarbon
HFID	Heated flame ionization detector
HMMWV	High Mobility Multipurpose Wheeled Vehicle
HO_2	Hydroperoxy radical
HRD	Hydrotreated renewable diesel
HRJ	Hydrotreated renewable jet fuel
HRR	heat release rate
HVO	hydrogenated vegetable oil
IGD	ignition delay
IMEPg	gross indicated mean effective pressure
JP-5	military jet fuel
LFE	laminar flow element
LHV	lower heating value
LLNL	Lawrence Livermore National Laboratory
NDIR	non-dispersive infrared

NO	nitric oxide
NTC	negative temperature coefficient
O_2	Oxygen
phi or φ	fuel air equivalence ratio
PP	peak pressure
QOOH	Alkyl peroxides
R	Alkyl radical
RO_2	Alkyl peroxy radical
ROHR	rate of heat release
RPM	revolutions per minute
SOC	start of combustion
SOI	start of injection
tau or τ	time delay
TC	top-center

INTRODUCTION

First generation bio-diesel fuels have been available for over a decade. These bio-diesel fuels have been frequently produced from rapeseed or soybean oils by chemically reacting the vegetable (or animal based) oil with methanol and a catalyst (*KOH*) to produce mono-alkylesters from the fatty acids present in the oil [1]. While the renewable nature of bio-diesel is attractive, its marginal stability and cold flow properties are significant challenges. In addition, susceptibility to water-based biocontamination could pose major problems for any water-based operational environment (e.g. maritime diesels).

Alternative diesel and jet engine fuels produced from hydrotreated renewable sources have begun to receive attention in recent years [2] with the resulting fuel having a paraffinic base. Hydrotreated Vegetable Oil (*HVO*) fuels come from renewable feedstock oils that are then hydrotreated and refined to produce a fuel that has similar molecular structure to Fisher-Tropsch fuels [3]. The absence of aromatics and cyclo-alkanes clearly aids in raising the cetane number of FT fuels [4] as well as *HVO* based fuels [5]. The US Navy is looking into Hydrotreated Renewable algae oil as a Diesel fuel replacement (*HRD*) as well as Hydrotreated Renewable camelina oil (*Camelina sativa*) as a Jet fuel replacement (*HRJ*). Jet fuel is used in some military diesel engines. These HVOs are not the ester based 'bio-diesel' of recent years, but rather pure paraffinic hydrocarbon fuels with no molecularly bound oxygen.

Due to its unique operational requirements as well as the lack of published technical data, the Navy is currently broadly evaluating two HVOs. The Navy is developing an all inclusive generic test and certification protocol that can be used to evaluate these potential alternative fuels for tactical Naval use. This study includes evaluating the basic properties of these alternative fuels in order to ensure a potential future fuel meets military specification and fit for purpose requirements. If these basic requirements are met, the Navy will then move forward with larger scale tests, such as testing the performance with fuel distribution and propulsion system components, and finally move to full-scale testing of the entire propulsion system. The goal of this certification process is to root out any anomalies in fuel chemistry or performance that would make it unsuitable for naval use.

As part of this Navy effort, the authors have tested both a *HRD* fuel from algae and a HRJ fuel from camelina in a conventional military 'Humvee' (*HMMWV*) diesel engine [6, 7]. Besides these published results, it is interesting that very little other published engine research data exists using these *HVO* fuels. The higher cetane nature of this fuel generally leads to shorter ignition delays with correspondingly longer overall burn durations with lower peak cylinder pressures. Overall however, the combusiton performance, while modestly different, has been acceptable. Engine brake metric differences of up to ten percent have been observed using these new fuels.

While the operational performance of these new *HVO* fuels was acceptable in the 'Humvee' engine, other Navy engines have very different engine geometry, fuel injection systems, and operating speed-load maps. It would be cost prohibitive to test a new fuel option in every possible application. Thus, due to the high cost involved in full-scale large marine engine testing, it would be advantageous to be able to predictively model the performance of a new fuel in a variety of existing engines. The challenge, however, is the complex nature of conventional diesel engine fuels and combustion.

Fortunately, new *HVO* fuels have a simpler structure as compared to conventional petroleum fuels, and this fact may allow combustion modeling to be pursued with reasonable fidelity. As mentioned above, *HVO* fuels have only paraffinic hydrocarbon components, lacking aromatics, cyclo-paraffins, and olefins which are standard components in conventional fuel. Combustion researchers have advanced both detailed and reduced chemical kinetic mechanisms for paraffinic hydro-carbon compounds, thus modeling their combustion performance in a diesel-like setting appears promising.

In this work, the authors compare experimental results from operation of a pure paraffinic fuel (single component) in a typical military diesel engine with the predictive results from a simple model based in chemical reaction kinetics. Clearly diesel combustion is a complex multiphase, unsteady, reacting turbulent flow system which makes predictive modeling difficult, particularly across many types and sizes of engines. However, the authors believe that a more simple view of focusing analytically on ignition delay can produce reasonably accurate indicators of acceptable engine performance. Thus, the authors here focus only on ignition delay and develop a simple constant pressure reactor model coupled with detailed chemical kinetics to capture the Start Of Combustion (*SOC* - e.g. ignition delay).

From previous work [8], the authors have shown that if the start of combustion (e.g. ignition delay) occurs within a modestly-sized 'window' of time after injection, then the engine will successfully operate and likely show reasonable combustion metrics. However, ignition delay that is outside this operational window will not result in viable engine operation. In other words, to first order, many important diesel engine combustion metrics can be tied closely with ignition delay. Since a large component of ignition delay is derived from a chemical induction period, as a first approach to evaluate the suitability of a new fuel, chemical kinetic modeling of the new fuel can lead to valuable insights.

Thus the objective of this paper is to show how a relatively simple model based in detailed chemical kinetics can be utilized to elucidate and, to first order, predict corresponding trends in ignition delay. To this end, a typical and legacy military diesel engine was utilized with a pure paraffinic fuel (single component) fuel, n-hexadecane. The overall purpose is to demonstrate how low-cost modeling could be utilized to assess the viability of candidate future fuels across a variety of legacy diesel engines.

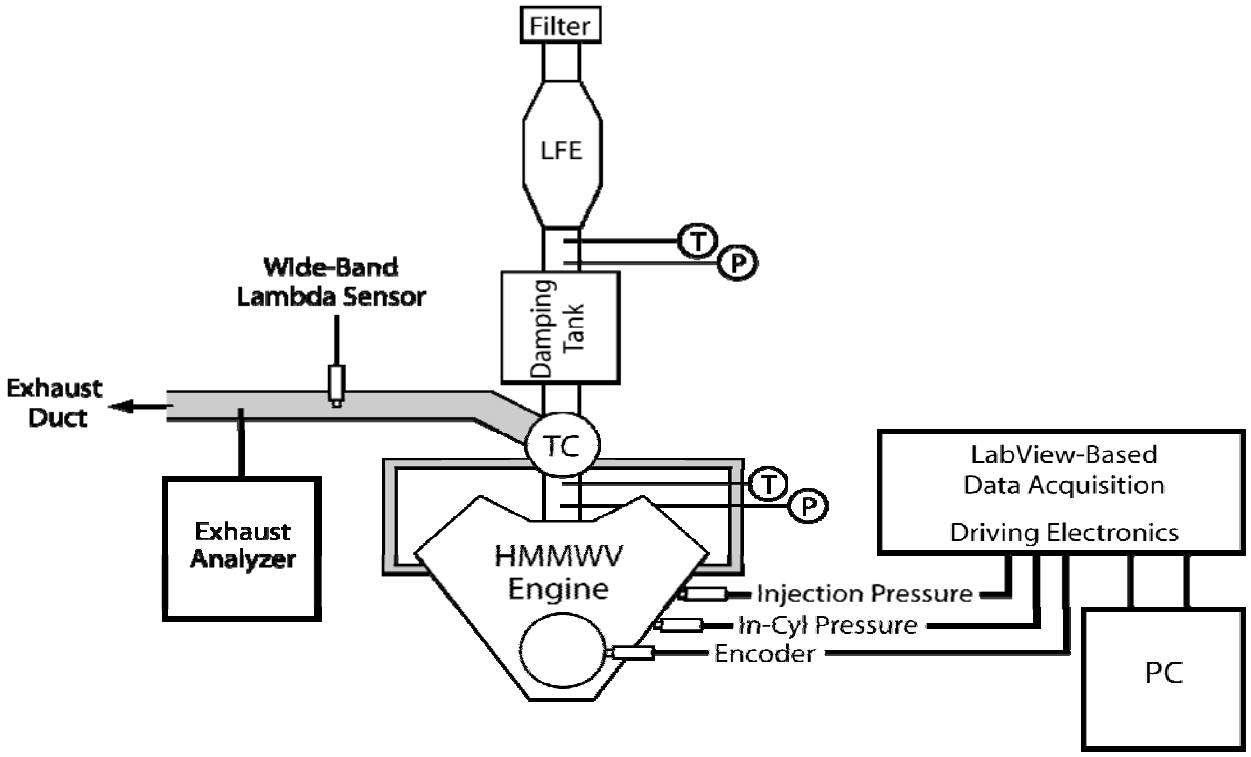

Figure 1: *HMMWV* engine experimental setup.

EXPERIMENTAL SETUP

The engine used in this study is an AM General Engine Products™ (*GEP*) 6.5 L V-8 *HMMWV* "Humvee" turbocharged diesel engine, manufactured in 2007. The engine is an indirect injection diesel with no electronic control in order to maximize reliability and durability in the field. It is equipped with 150-bar single hole injectors. Table 1 lists the basic specifications of this engine and the operating conditions used in this study. A Kistler™ 6056 pressure transducer was mounted in the

engine head (cylinder #1 only) and used in conjunction with a Kistler™ 5010B charge amplifier. A Kistler™ 4046 fuel line pressure transducer was utilized to determine start of injection. Airflow was measured with a Meriam™ laminar flow element. A BEI™ 2-channel shaft encoder with crank angle degree resolution and TC pulse was used for engine crankshaft position indicating. A line diagram of the engine configuration is shown in Figure 1. Data were collected with a National Instruments™ LabView data acquisition system sampling at a rate of 50 kHz. Approximately 100 engine cycles were collected at a given engine operating condition.

Table 1: Experimental engine parameters.

Type	Indirect-injection diesel
Bore	103 mm
Stroke	97 mm
Maximum Power	142 kW at 3600 RPM
Maximum Torque	522 Nm at 1800 RPM
Compression Ratio	21 (manufacturer spec.)
Coolant	water cooled
Intake Air	turbocharged, 0 – 7 psig boost
Fuel	n-hexadecane (cetane)

	$nC_{16}H_{34}$

Exhaust gas was analyzed using a steady-state analyzer system and sampled from the exhaust flow using a heated filter approximately 10 cm downstream of the exhaust port. Hydrocarbons (*HC*) were measured on a wet basis using a CAI™ model 600 heated flame ionization detector (*HFID*). Oxygen (O_2), carbon dioxide (CO_2), and carbon monoxide (*CO*) were measured with a CAI™ model 602P combined non-dispersive infrared absorption (NDIR) and paramagnetic sensor. Nitric oxide (*NO*) emissions were measured using a CAI™ model 600 heated chemiluminescent analyzer on a dry basis. An ETAS™ LA4.2 wide-band oxygen sensor was used to measure the air-fuel ratio at all operating conditions; combined with the air-flow measurement, this measurement allowed calculation of the fuel flow rate.

EXPERIMENTAL BRAKE RESULTS

Data were collected at approximately twenty speed-load operating points. In the following figures these experimental data are reported as contour lines on a plane of fuel-air equivalence ratio, phi (φ) plotted on the horizontal axis with the engine speed (*RPM*) on the vertical axis.

Figure 2 shows the Brake Mean Effective Pressure (*BMEP*) performance of the Humvee engine across the equivalence ratio-speed map. It can be seen that the equivalence ratio is roughly proportional to the engine's *BMEP*, thus the horizontal-axis, phi (φ), approximately represents engine load.

For a given engine speed, *BMEP* increases with φ due to the increased fueling per cycle. At a given equivalence ratio, *BMEP* decreases modestly with increasing speed due to the increased importance of friction with increasing speed. The maximum *BMEP* running cetane is approximately ten percent lower than engine operation on diesel fuel due to the reduced density of cetane (0.77 v. 0.86 specific gravity) since the fuel injection pump delivers a fixed maximum volume of fuel at maximum load. Corresponding maximum engine power is down approximately ten percent (130 v. 143 *kW*) running the engine with pure cetane fuel.

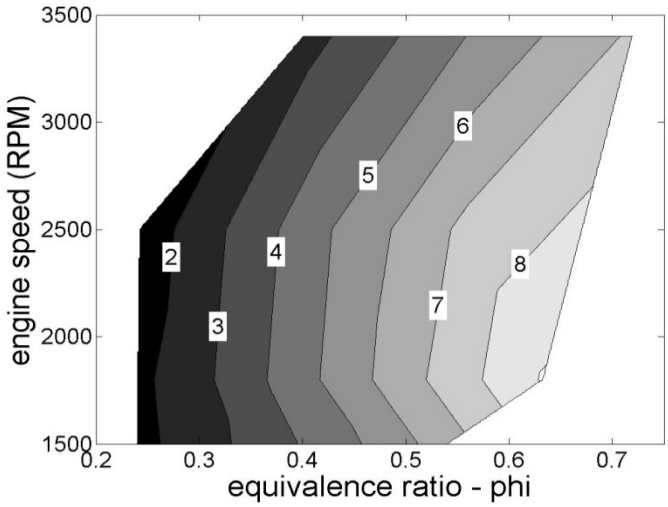

Figure 2: *BMEP* (bar) for operation with nC16

Figure 3 shows the Brake Specific Fuel Consumption (*BSFC*) characteristics of the Humvee engine running cetane fuel. For a given engine speed, *BSFC* improves with increasing φ. This result is due to the nearly constant *FMEP* (Friction Mean Effective Pressure) friction behavior of the engine at a

given speed. Thus the relative importance of friction diminishes as load increases at a given engine speed. As engine speed increases *BSFC* worsens (increases) due to increasing engine friction.

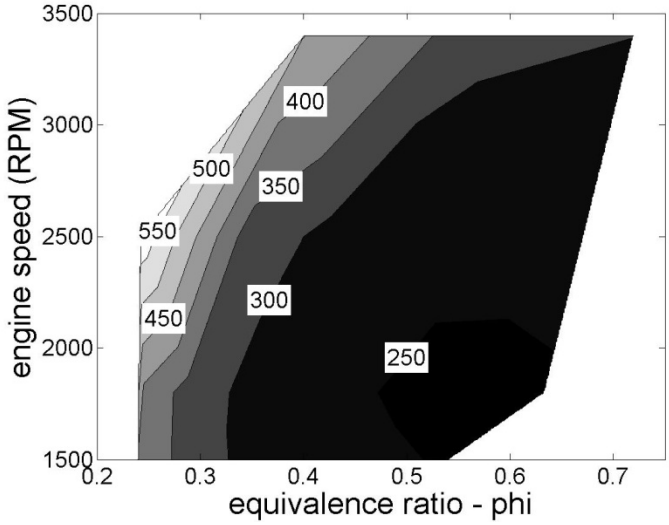

Figure 3: Brake Specific Fuel Consumption (*BSFC*) for Humvee engine operation on nC16 (gm/kW-hr).

EXPERIMENTAL IGNITION DELAY

A conventional engine heat release analysis modeled after MIT's Single Zone approach [9, 10, 11] was used to further analyze the engine's in-cylinder pressure data. This single zone model uses a first-law energy balance with combined unburned and burned single zone average properties to determine the rate of energy release. The latent heat of fuel vaporization was not included in this heat release analysis. As this is a legacy (low-pressure) mechanically injected engine, the fuel injection event is characteristically twice as long as the ignition delay period, thus the authors believe that combustion begins before the majority of fuel has been injected and vaporized. Fast data

sampling was converted to crank angle degrees and engine wall heat transfer was accomplished with the conventional instantaneous spatially averaged Woschni coefficient. This analysis is useful to characterize start of combustion and burn durations. Start of injection (*SOI*) was determined from an injector pressure sensor. Start of combustion (*SOC*) was determined analytically as the 5% rise in instantaneous heat release above the *SOI* level. Ignition delay was then determined experimentally as the difference between *SOI* and *SOC*. A sample of these results is shown in Figure 4 for the 1500 *RPM*, lightest load case. Experimental in-cylinder pressure and injector fuel line pressure data are also shown in this figure. *SOI* is seen to occur at 348° (12° *BTC*) and is denoted by the left most dashed vertical line. *SOC* as determined by the 5% of maximum *HRR* (instantaneous Heat Release Rate) occurs at 351° (9° *BTC*) is shown by the next vertical dashed line. Thus ignition delay is determined to be the difference of *SOC* and *SOI*, which for this operating condition is 3 crank angle degrees (*CAD*).

It should be noted that in-cylinder pressure was measured in the pre-chamber of this HMMWV engine. The HMMWV pre-chamber is the principle combustion chamber volume of the engine (only a small dish exists on the piston crown) with a relatively large and short passageway (cross-sectional area of approximately 1 cm^2 with transfer tube less than 1 cm in length) that connects the pre-chamber to the main engine cylinder. It is possible that a small pressure difference could exist between the pre-chamber and the main chamber during periods of high pre-chamber flow (e.g. mid-intake-stroke and during the bulk burn), however, that is expected to only modestly affect IMEP calculations and not the heat release analysis which is the focus of this study.

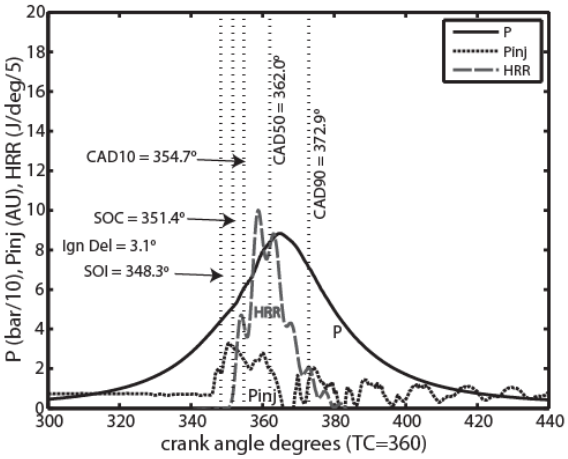

Figure 4: Heat release analytical results at 1500 *RPM*, light load.

Figure 5 shows a summary of ignition delay (*IGD*) characteristics on a time basis (msec) across the speed-load map running with cetane fuel operation. It can be seen that at a given engine speed, *IGD* decreases modestly (shortens) with increasing load. Experimental variability in the determination of IGD is modest, especially at lower engine speeds, and will be shown as confidence intervals bars in a following figure. Heywood [11] describes *IGD* decreasing with load due to residual gas and engine wall temperature increases with increasing load. Further, *IGD* decreases at a given φ with increasing engine *RPM* due to the higher in-cylinder pressures and temperatures at *SOI*, as will be shown shortly.

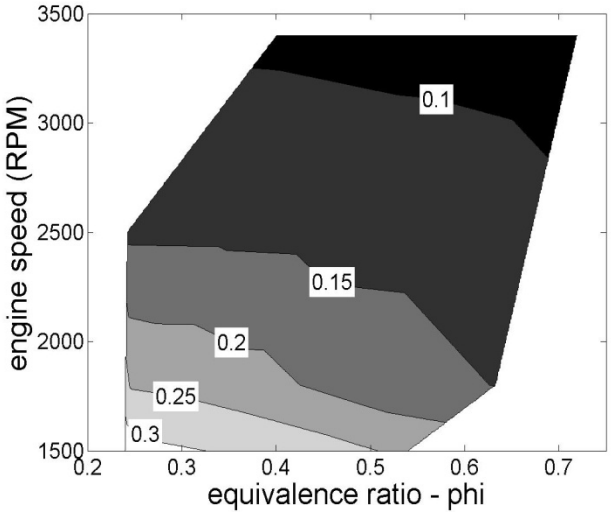

Figure 5: Experimental ignition delay (msec) results for the Humvee engine operating on nC16.

IGNITION DELAY MODELING

Conceptually, total experimental *IGD* can be broken down into two steps comprised of a physical delay period and a chemical delay period. This approach has been described in Ref. [1] with the caveat that some overlap exists between the physical delay and the chemical delay. For this study these two delay periods will be assumed, to a first order, to be distinct and sequential. The physical delay portion (τ_{phys}) of this model includes the time required for a fuel spray to leave the injector, form droplets and entrain hot air, vaporize, mix, and reach a critical temperature required for the onset of rapid chemical reaction. These steps may all be occurring simultaneously and are depicted, along with associated fuel properties, in Ref. [8]. Next, the chemical ignition delay period (τ_{chem}) includes the time required to initiate the chemical reactions that will quickly lead to explosive radical chain branching.

In the forthcoming analysis, the physical delay period will be determined as the difference between experimental total ignition delay (τ_{ign}) and the model predicted chemical ignition delay (τ_{chem}), to be described in detail in the next section. The authors pursued this approach in a previous technical paper (see Ref. [13]), comparing experimental *IGD* results to chemical kinetic IGD (τ_{chem}) modeling results (also using a constant pressure reactor approach with SOI conditions) at a single engine speed and load running a binary surrogate fuel. For this study, the approach of measuring τ_{ign} and modeling τ_{chem} is applied across the engine's entire speed-load range to determine τ_{phys}. It is the hope of the authors that current and future experimental and modeling based diesel spray research will be able to provide an alternative path to determine τ_{phys} so that a complete analytically-based initial evaluation of a new fuel's acceptability can be pursued.

CHEMICAL DELAY PERIOD

Once a fuel-vapor and air mixture is obtained with suitable temperature and mixture ratio for chemical reaction (to be discussed further in the next section), there is a chemical delay period during which chemical reaction rates increase, ultimately leading to significant fuel chain branching. At high temperatures the main chain branching reactions involve H radicals reacting with molecular oxygen to form *OH* plus *O*; when the temperature is lower though, the chemistry of hydroperoxides is dominating and around 900*K* the main source of radicals is the rapid decomposition of H_2O_2 into two *OH* radicals. Although the addition of alkyl radicals (*R*) to molecular oxygen (O_2) occurs at a slightly lower temperature, it also leads to degenerate chain branching and is extremely important to predict the onset of ignition in low- and moderate-temperature combustion systems such as diesel combustion [12]. Low temperature chain branching occurs in a several step process, the first being an

alkylperoxy (RO_2) isomerization step, in which a peroxy group abstracts an *H* from the chain through a ringed transition state:

$$RO_2 \rightarrow QOOH \qquad (1)$$

The rate of this isomerization step depends on the size of the ringed transition state and the type of *C-H* which is broken by the abstraction. For long chain alkane species (e.g. cetane), there are many possible routes for this isomerization step, and thus the overall rate is faster than for shorter chain length species. The time required for these and subsequent steps to yield significant chain branching is the main component of the chemical delay.

In order to more completely address the split between physical and chemical delay periods, the chemical delay period was computer modeled using an approach similar to that found in Refs. [14, 15 and 16]. Ignition delay was modeled using a homogeneous constant pressure reactor assumption with a wide range of equivalence ratios (2-10) in order to evaluate ignition delay effects across a broad range of fuel-air mixtures. Initial conditions were chosen to be the in-cylinder pressure and temperature at *SOI* for each operating condition as shown in Figure 6 and Figure 7 which is indicative of the environment into which the fuel is injected in the experimental engine. The temperature at *SOI* was determined using the above described heat release analysis. Chemical *IGD* (τ_{chem}) was defined as the time from the start of reaction modeling to when the rate of change of temperature reached its maximum (e.g. explosive chain branching). Other criteria based on specific species concentrations have been used, with all of these approaches providing very similar predicted chemical *IGD* times.

The detailed *LLNL* chemical kinetic model for n-hexadecane was assembled by combining previously developed mechanism for large n-alkanes. The mechanism for large n-alkanes considers n-alkanes up to n-hexadecane [15]. It includes both low and high temperature chemistry so that it can simulate ignition over the entire temperature range for diesel combustion. It has been validated for ignition over a wide range of temperatures, pressures and equivalence ratios. To create the present mechanism, the species and reactions necessary to model the C8 to C16 n-alkanes [15] were used.

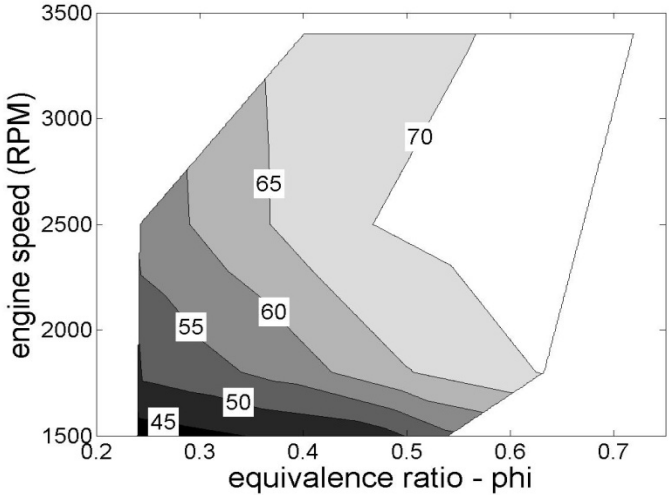

Figure 6: In-cylinder pressure (bar) at *SOI*.

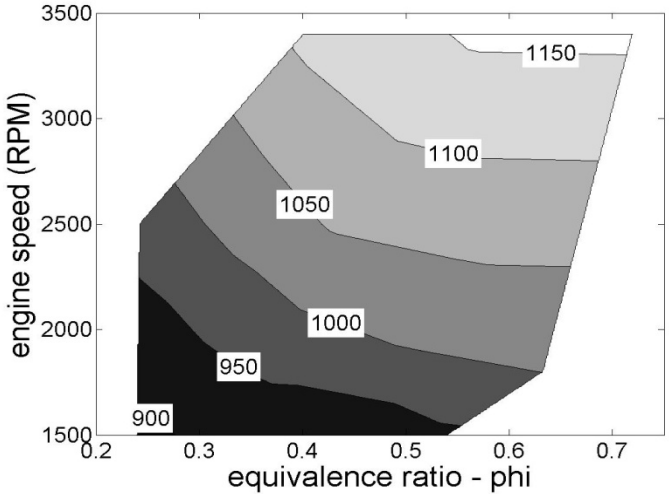

Figure 7: In-cylinder temperature (K) at *SOI* using heat release analysis model.

CHEMICAL IGNITION DELAY MODELING RESULTS

The initial modeling effort involved simulating the chemical ignition delay using various fuel-air equivalence ratios (φ) in order to better understand the sensitivity. Results shown at the five different 1500 *RPM* load points are shown in Figure 8. The solid black bar with each data set is the experimentally measured total ignition delay. The additional five gray scale bars in each data set are the *LLNL* model-predicted chemical *IGD* at equivalence ratios from 2 to 6. Note that the general trend of decreasing chemical *IGD* with increasing load is captured by the model in agreement with the experimental data.

The chemical delay is significantly shorter than the total experimental *IGD*. As described earlier, this difference is the physical delay time for the spray to develop a combustible mixture. It can also be seen that $\boldsymbol{\varphi}$ = 4 provides the shortest-quickest *IGD*. In Figure 9 is shown the 1500 *RPM* data from Figure 8 as well as the experimental and modeling results for the three 3400 *RPM* operating points. The modeling results with various equivalence ratios at 1800 and 2500 *RPM* were removed for figure

clarity, but follow the same general trends as the low and high speed cases. Again it can be seen that for the high speed (3400 *RPM*) points, an equivalence ratio of four has the shortest *IGD*. An equivalence ratio of six can be seen to be unlikely for the first fuel-air parcel to ignite, since the model-predicted result exceeds the experimentally measured total IGD. Representative experimental 95% confidence intervals are shown for both a low speed and high speed case.

Since this study is investigating *IGD* and *SOC*, the quickest chemical delay fuel-air parcel (φ = 4) is thus most important as it will determine when combustion begins. This equivalence ratio will be the focus of the rest of this study, and is also consistent with previous work 17.

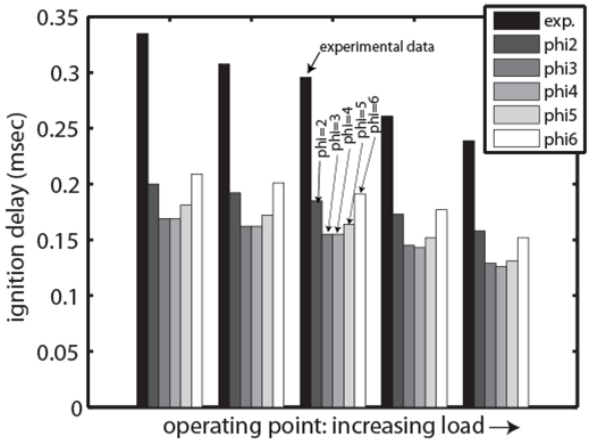

Figure 8: 1500 *RPM* ignition delay modeling with various equivalence ratios (φ).

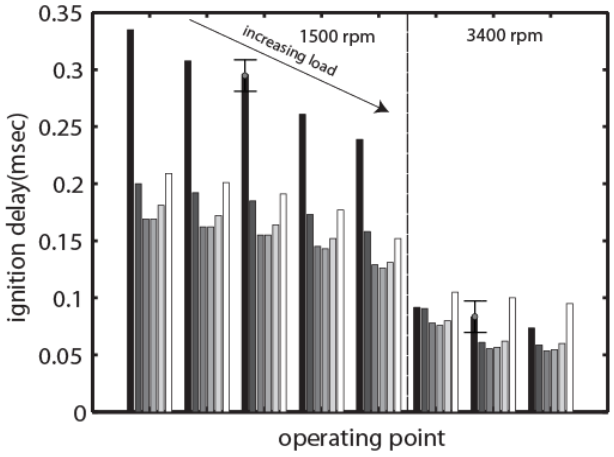

Figure 9: Ignition delay modeling results at 1500 *RPM* and 3400 *RPM*.

Both experimental and model predicted chemical ignition delays are shown in Figure 10 for all of the speed-load points. It should be noted that no chemical kinetic model calibration was pursued in this study. *LLNL's* long-chain alkane mechanism was applied directly to the Humvee operating conditions. Overall the model predicts the general trends of the experimental data remarkably well. *IGD* delay is shorter with increasing load at a given speed. *IGD* is also shorter with increasing speed. The model captures both of these effects. The moderate difference between the experimental data and the model predicted chemical IGD is due to the physical delay time discussed above. The resulting τ_{phys} will be discussed later on in this paper.

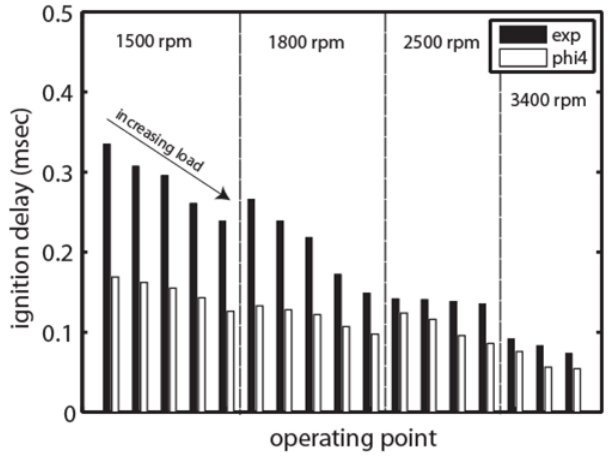

Figure 10: Ignition delay modeling results across the speed-load range.

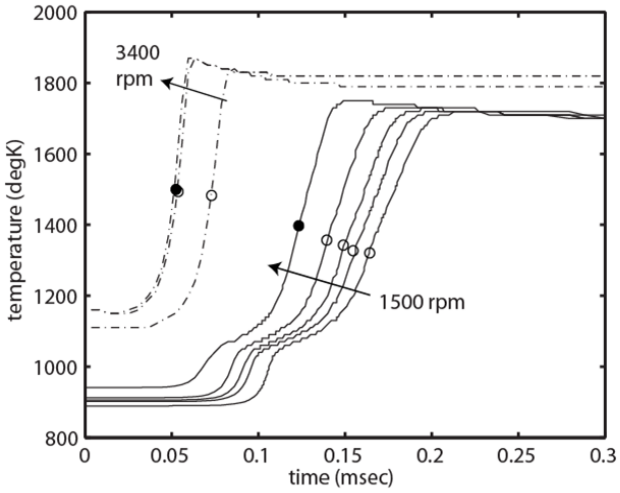

Figure 11: Model-predicted temperature at 1500 and 3400 *RPM*.

The detailed chemical kinetic model predicted temperature histories of the φ=4 fuel-air packet is shown in Figure 11 for the low and high speed cases. It is important to recall that the initial temperature for each operating point was based on *SOI* conditions at each individual operating point. Thus, the 3400 *RPM* cases are significantly hotter at *SOI* and are shown as dashed lines in the figure. The solid lines are the 1500 *RPM* data and are cooler due to the increased time for heat

transfer each engine cycle. For each speed data set an arrow shows the direction of increasing load. This indicating arrow label will be used in following data figures as well. Additionally shown on this figure (and following figures) are two black 'dots'. These show the ignition point using the $(dT/dt)_{max}$ ignition criterion described above. The additional open circle symbols show, just for this figure, the ignition points for the other load points in each engine speed data set. It can be seen that ignition occurs in the 1300 to 1500 *K* range characteristic of heavy hydrocarbon fuels. The open symbols will be left off in future figures in order to improve figure clarity.

The modeled temperature behavior in Figure 11 shows an interesting two step trend. This behavior is due to the Negative Temperature Coefficient (*NTC*) region behavior that characteristic of straight chain alkanes reacting in the 800 to 1000 K region. This *NTC* temperature regime is slightly higher than that normally seen from laboratory combustion studies, however these results are consistent with a recent research from *LLNL* [18]. This region has been shown to be important for straight chain alkanes where endothermic reactions delay kinetics. In this temperature regime, alkylperoxy fuel radicals (RO_2) become unstable preventing the low temperature degenerate chain branching from taking place, leaving the hydroperoxyl radical (HO_2) and hydrogen peroxide (H_2O_2) decomposition to control the reactivity. At these lower temperatures, characteristic of the end of compression combustion chamber environment at lower engine speeds, the dominant kinetic paths takes place primarily through the formation of alkyl-peroxy radicals (RO_2) via addition of molecular oxygen to alkyl (*R*) radicals, followed by production of alkyl hydroperoxides (*QOOH*). Additionally it can be seen that the high speed cases (3400 *RPM*) do not show this two-stage *NTC* type behavior. This is because the temperature of the combustion chamber at *SOI* is well above 1000 *K* for the 3400 *RPM* operating

points. Thus, the chemical kinetics are driven by more dominating high temperature reactions that do not display *NTC* characteristics.

Next is shown how the fuel ($nC_{16}H_{34}$: normal n-hexadecane) is consumed in this reacting fuel-air parcel. Figure 12 shows the n-hexadecane fuel mole fraction (concentration) as a function of time for the operating points at both 1500 and 3400 *RPM*. Again an arrow is placed across each engine *RPM* data set to show the trends with increasing load. Additionally the ignition 'dots' are placed at the time of ignition for only the highest load operating point at each speed. By the time ignition occurs, essentially all of the fuel has been consumed leading to combustion (the ignition 'dots' are essentially on the horizontal axis). The 3400 *RPM* fuel consumption histories show a steady depletion in base fuel ($n\text{-}C_{16}H_{34}$) as the fuel is breaking down ultimately to form *CO*, CO_2 and H_2O The 1500 *RPM* cases, show the two-stage *NTC* behavior as described above, which slows down the rate of fuel consumption due to the endothermic chemical kinetics early in the reaction process.

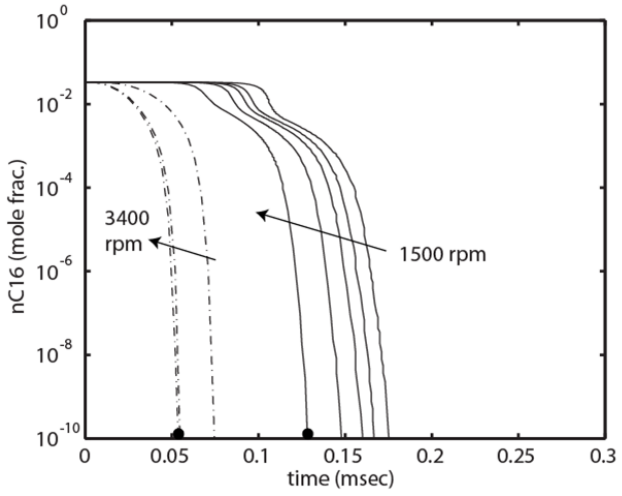

Figure 12: Fuel $nC_{16}H_{34}$ (n-hexadecane) concentration history.

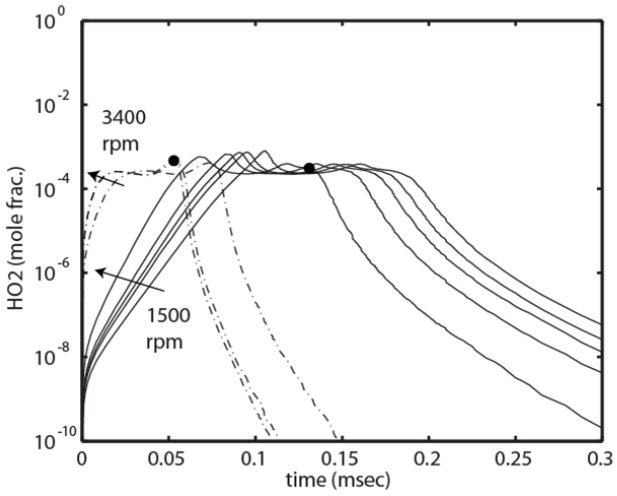

Figure 13: HO_2 (hydroperoxy) radical concentration history.

As hydrogen atoms are extracted from the fuel, two key radicals are formed, HO_2 and H_2O_2, that further allow the chemical reactions to proceed. The detailed chemical kinetic model provides detailed insights into these early reactions leading to combustion. Figure 13 shows the formation of the hydroperoxy radical (HO_2). This radical can be formed by the concerted elimination reaction ($ROO \rightarrow$ Olefin+HO_2) or by the addition of O_2 to a hydrogen atom that was recently eliminated by partially oxidized fuel fragments. It can be seen that HO_2 builds up to a quasi-steady level before ignition-combustion is defined to occur. HO_2 based reactions are thus important throughout the entire chemical induction (chemical *IGD*) period.

Hydrogen peroxide (H_2O_2) formation is next shown in Figure 14. H_2O_2 is a strong oxidizer that can aid in further fuel decomposition. During the early phases of the kinetics, once the fuel vapor and air mixture have formed, H_2O_2 comes principally from reactions of fuel with HO_2. Hydrogen peroxide also comes from the reaction of two HO_2 molecules leading to H_2O_2 and O_2. It can be seen from the two combustion 'dots' (both at 3400 and 1500 *RPM*) that H_2O_2 builds up to a maximum concentration

midway through the chemical induction period (chemical *IGD* period) and after the H_2O_2 has dissociated (e.g. reduced in concentration) into OH radicals does combustion finally occur.

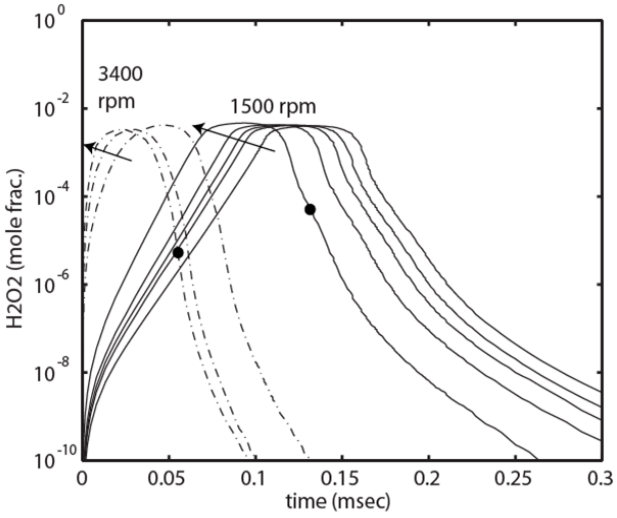

Figure 14: H_2O_2 (hydrogen peroxide) concentration history.

The three important intermediate species, hydroxyl radical (*OH*), the late forming acetylene (C_2H_2), and high temperature formaldehyde (CH_2O) develop as is characteristic of pure hydrocarbon combustion. These will be shown in composite specie summary figures later in this paper.

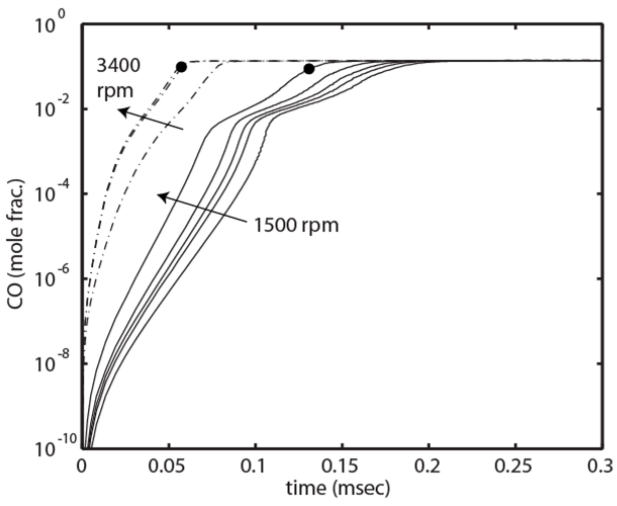

Figure 15: *CO* (carbon monoxide) concentration history.

Carbon monoxide formation is the next to final step in hydrocarbon oxidation of a stoichiometric fuel-air parcel. However, for fuel rich combustion *CO* can be a stable final product as is shown in Figure 15. The concentration of *CO* is seen to be at approximately ten-percent at the time of ignition, and holds steady after combustion begins.

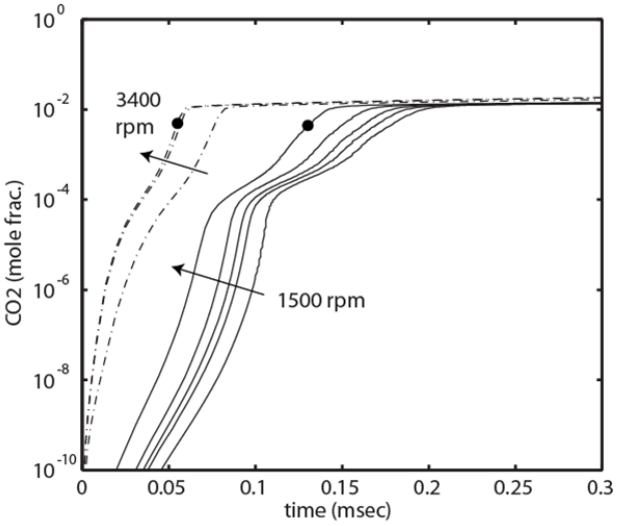

Figure 16: *CO_2* (carbon dioxide) concentration history.

Carbon dioxide formation principally comes from the further oxidation of *CO* provided that sufficient oxygen is present. *CO_2* levels are seen to be well below one-percent at the time of ignition, peaking at only 1-2% overall when combustion is allowed to progress completely. This concentration is an order of magnitude lower that what is formed during stoichiometric hydrocarbon combustion. This very low level of *CO_2* formation is due to the very rich fuel-air packets that are first to ignite in a diesel flame.

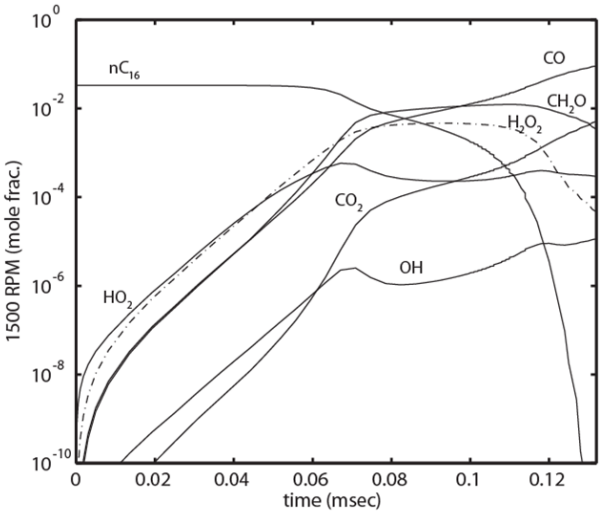

Figure 17: 1500 *RPM* (high load) composite species behavior leading up to ignition at 0.13 msec.

Finally, composite species histories are shown for both the low speed and high cases (high load). The results for 1500 RPM are shown in Figure 17. It can be seen that early in the fuel-air kinetics that HO_2 formation rates are greater than that of H_2O_2. However H_2O_2 formation mechanisms begin to dominate at approximately 0.06 msec. The *NTC* behavior is also now clearly evident at nominally 0.07 msec after the start of the kinetics. This *NTC* behavior tends to slow down the progression of the reactions leading to ignition. A reduction in *OH* and HO_2 is seen during this period which is why the cooler 1500 *RPM* cases take longer to ignite.

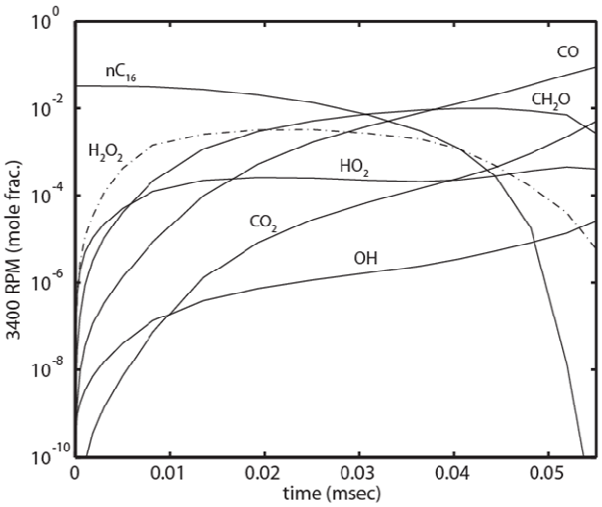

Figure 18: 3400 *RPM* (high load) composite species behavior leading up to ignition at 0.55 msec.

The composite history of the key species for 3400 *RPM* (high load) is shown in Figure 18. It can be seen that due to the high temperature initial temperature that the reactions proceed directly into high temperature kinetic paths and thus no *NTC* behavior is seen which tends to delay the progression towards ignition. This high speed case leads to fast combustion.

PHYSICAL DELAY PERIOD

A mid-load summary of the ignition delays as a function of engine speed is shown in Figure 19. The top data line represents the total-experimentally measured IGD. The chemical ignition delay (τ_{chem}) is the model predicted delay and is represented by the dark gray region. The physical delay is the difference of the total and chemical delays and is represented by the light gray region. The total *IGD* is the sum of the physical and chemical delays. As discussed throughout this paper, the total *IGD* decreases with engine speed. Note also that the chemical ignition delay decreases with increasing

engine speed, although at a more modest rate. This analysis shows and suggests that the physical delay is the most sensitive to engine speed, decreasing inversely with engine speed. As engine turbulence length scales also decreases inversely with engine speed, this effect is qualitatively physically correct. Knowledge of this physical delay time could be used with future chemical kinetic modeling results from different fuels (or fuel surrogates) to predict total ignition delay of a new fuel in an effort to determine fuel suitability. The authors are also pursuing model based research in order to analytically predict this physical delay time in the engine context.

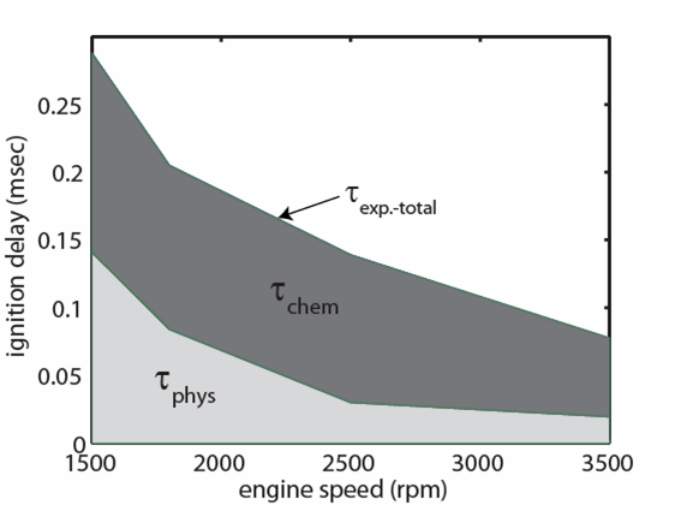

Figure 19: Mid-load summary of total *IGD* as well as the physical and chemical delays.

CONCLUSIONS

The following conclusions can be drawn from this experimental and modeling study running pure paraffinic ($nC_{16}H_{34}$) fuels in a legacy military diesel engine:

- Total experimental ignition delay is seen to shorten with both increasing engine load and increasing engine speed.
- The chemical *IGD* delay period (chemical ignition delay) as modeled using detailed *LLNL* kinetics using initial conditions reflecting SOI conditions also show shorter (decreasing) ignition delays with increasing engine load and speed.
- The chemical delay periods were consistently shorter than the experimental ignition delays, showing that a physical delay period from the diesel spray accounts for the difference.
- The analytically determined physical delay period is a minority fraction of the total ignition delay time across the speed-load range, and the reduction of the physical delay period with increasing speed is consistent with increased mixing due to enhanced turbulence.
- The approach used within this study is promising for predicting the ignition delay (and start of combustion) to predict viability of candidate future fuels in legacy diesel engines.

REFERENCES

1 **Challen and Baranescu**, Diesel Engine Reference Book, SAE, 1999.

2 **Kuronen, M., Mikkonen, S., Aakko, P. And Murtonen, T.,** "Hydrotreated Vegetable Oil as Fuel for Heavy Duty Diesel Engines", 2007, SAE Technical Paper #2007-01-4031.

3 **Aatola, H., Larmi, M., Sarjovaara, T. and Mikkonen, S.,** "Hydrotreated Vegetable Oil (HVO) as a Renewable Diesel Fuel: Trade-off between NOx, Particulate Emission, and Fuel Consumption of a Heavy Duty Diesel Engine", 2008, SAE Paper #2008-01-2500.

4 **Kitano, K, Sakata, I. and Clark, R.,** "Effects of GTL Fuel Properties on DI Diesel Combustion", 2005, SAE Paper#2005-01-3763.

5 **Shonnard, D.R., Williams, L. and Kalnes, T.N.,** "Camelina Derived Jet Fuel and Diesel: Sustainable Advanced Biofuels", Environmental Progress and Sustainable Energy, 2010, Vol. 29, No. 3.

6 **Hamilton, L.J., Williams, S.A., Kamin, R.A., Carr, M.A., Caton, P.A. and Cowart, J.S.,** "Renewable Fuel Performance in a Legacy Military Diesel Engine", August 2011, Proceedings of the 2011 Energy Sustainability Conference (paper #ESFuelCell 2011-54101), Washington DC.

7 **Caton, P.A., Williams, S.A., Kamin, R.A., Luning-Prak, D., Hamilton, L.J., and Cowart, J.S.,** "Hydrotreated Algae Renewable Fuel Performance in a Military Diesel Engine", May 2012, Proceedings of the 2012 ASME Spring Internal Combustion Engine Conference (paper #ICES 2011-81048), Torino, Italy.

8 **Caton, P. A., Hamilton, L. J., and Cowart, J. S.,** “Understanding Ignition Delay Effects with Pure Component Fuels in a Single Cylinder Diesel Engine,” ASME Journal of Gas Turbines and Power, 2010, in press.

9 **Gatowski, J.A., Balles, E.N., Chun, K.M., Nelson, F.E., Ekchian, J.A., Heywood, J.B.,** “Heat Release Analysis of Engine Pressure Data”, 1984, SAE #841359.

10 **Chun, K.M. and Heywood, J.B.,** “Estimating Heat Release and Mass of Mixture Burned from SI Engine Pressure Data”, Combustion Science and Technology, 1987, Vol. 54, pp. 133-143.

11 **Heywood, J.B.,** Internal Combustion Engine Fundamentals, 1988, Mc-Graw Hill.

12 **Westbrook, C.K., Pitz, W.J., Herbinet, O., Curran, H.J. and Silke, E.J.,** "A Detailed Chemical Kinetic Reaction Mechanism for n-Alkane Hydrocarbons from n-Octane to n-Hexadecane," *Combust. Flame,* 2009, 156 (1) 181-199.

13 **Carr, M.A., Caton, P.A., Hamilton, L.J., Cowart, J.S., Mehl, M. and Pitz, W.J.,** “An Experimental and Modeling Based Study into the Ignition Delay Characteristics of Diesel Surrogate Binary Blend Fuels”, October 2011, Proceedings of the ASME 2011 Internal Combustion Engine Fall Technical Conference (paper#ICEF2011-60027), Morgantown, WV.

14 **Curran, H. J., Fisher, E. M., Glaude, P. A., Marinov, N. M., Pitz, W. J., Westbrook, C. K., Layton, D. W., Flynn, P. F., Durrett, R. P., zur Loye, A. O., Akinyemi, O. C., Dryer, F. L.,** “Detailed Chemical Kinetic Modeling of Diesel Combustion with Oxygenated Fuels,” 2001, SAE Paper #2001-01-0653.

15 **Westbrook, C. K., Pitz, W. J., and Curran, H. J.,** "Chemical Kinetic Modeling Study of the Effects of Oxygenated Hydrocarbons on Soot Emissions from Diesel Engines," J. Phys. Chem. 2006, A, 110, 6912 – 6922.

16 **Sarathy, S.M., Westrook, C.K., Mehl, M., Pitz, W.J., Togbe, C., Dagaut, P., Wang, H., Oehlschlaeger, M.A., Nieman, U., Seshadri, K., Veloo, P.S., Ji, C. Egolfopoulos, F.N. and Lu, T.,** *Combustion and Flame* 158, 2011, 2338-2357.

17 **Dec, J.E.,** "A Conceptual Model of DI Diesel Combustion based on Laser Sheet Imaging", 1997, SAE Technical Paper #970873.

18 **Mehl, M., Pitz, W.J., Westrook, C.K. and Curran, H.J.,** "Kinetic Modeling of Gasoline Surrogate Components and Mixtures under Engine Conditions", 2011, *Proceedings of the Combustion Institute*, 33, pp 193-200.

19 **Westbrook, C.K. and Pitz, W.J.,** "Chemical Kinetic Modeling of Combustion of Practical Hydrocarbon Fuels", 1989, SAE Technical Paper #890990.

20 **Mehl, M., Pitz, W.J., Westbrook, C.K. and Curran, H.J.,** "Kinetic Modeling of Gasoline Surrogate Components and Mixtures under Engine Conditions," 2011, *Proc. Combust. Inst.* 33 (1) 193-200.

21 **Mathes, A., Reis, J., Caton, P.A., Cowart, J.S., Luning-Prak, D., Hamilton, L.J.,** "Binary Mixtures of Branched and Aromatic Pure Component Fuels as Surrogates for Future Diesel Fuels", 2010, *SAE International Journal of Fuels and Lubricants,* vol. 3, no. 2, pp. 794-809.

22 **Cowart, J.S., Carr, M.A., Caton, P.A., Stoulig, L., Luning-Prak, D., Moore, A., Hamilton, L.J.,** "High Cetane Fuel Combustion Performance in a Conventional Military Diesel Engine", 2011, *SAE International Journal of Fuels and Lubricants*, Vol. 4, No.2).

23 **Carr, M.A., Caton, P.A., Hamilton, L.J., Cowart, J.S., Mehl, M. and Pitz, W.J.,** "An Experimental and Modeling Based Study into the Ignition Delay Characteristics of Diesel Surrogate Binary Blend Fuels", Oct 2011, *Proceedings of the ASME 2011 Internal Combustion Engine Fall Technical Conference* (paper#ICEF2011-60027), Morgantown, WV.

CONTACT INFORMATION

Jim Cowart: cowart@usna.edu

ACKNOWLEDGMENTS

The authors wish to thank Dr. Sharon Beerman-Curtin and the Office of Naval Research (ONR) for their support of this work. Appreciation is also extended to Mr. Taylor Holland and AM General for providing the test engine. The work at LLNL was performed under the auspices of the U.S. Department of Energy by Lawrence Livermore National Laboratory under Contract DE-AC52-07NA27344.

List of Tables

Table 1: Experimental engine parameters.

List of Figure Captions

Figure 1: HMMWV engine experimental setup.

Figure 2: *BMEP* (bar) for operation with nC16

Figure 3: Brake Specific Fuel Consumption (*BSFC*) for Humvee engine operation on nC16 (gm/kW-hr).

Figure 4: Heat release analytical results at 1500 *RPM*, light load.

Figure 5: Experimental ignition delay (msec) results for the Humvee engine operating on nC16.

Figure 6: In-cylinder pressure (bar) at *SOI*.

Figure 7: In-cylinder temperature (K) at *SOI* using heat release analysis model.

Figure 8: 1500 *RPM* ignition delay modeling with various equivalence ratios (***φ***).

Figure 9: Ignition delay modeling results at 1500 *RPM* and 3400 *RPM*.

Figure 10: Ignition delay modeling results across the speed-load range.

Figure 11: Model-predicted temperature at 1500 and 3400 *RPM*.

Figure 12: Fuel nC16H34 (n-hexadecane) concentration history.

Figure 13: HO2 (hydroperoxy) radical concentration history.

Figure 14: H2O2 (hydrogen peroxide) concentration history.

Figure 15: *CO* (carbon monoxide) concentration history.

Figure 16: *CO2* (carbon dioxide) concentration history.

Figure 17: 1500 *RPM* (high load) composite species behavior leading up to ignition at 0.13 msec.

Figure 18: 3400 *RPM* (high load) composite species behavior leading up to ignition at 0.55 msec.

Figure 19: Mid-load summary of total *IGD* as well as the physical and chemical delays.